

RESEARCH ARTICLE | JULY 18 2023

Vibrational frequencies of CO bound to all three low-index cerium oxide surfaces: A consistent theoretical description of vacancy-induced changes using density functional theory

Pablo G. Lustemberg ; Chengwu Yang ; Yuemin Wang ; Christof Wöll  ;
M. Verónica Ganduglia-Pirovano  



J. Chem. Phys. 159, 034704 (2023)

<https://doi.org/10.1063/5.0153745>



CrossMark

Articles You May Be Interested In

Acoustic Streaming in the Vicinity of a Cylinder

J Acoust Soc Am (June 2005)

Acoustical Streaming in the Vicinity of a Sphere

J Acoust Soc Am (June 2005)

Acoustical Streaming in the Vicinity of a Cylinder

J Acoust Soc Am (June 2005)

Webinar

Boost Your Signal-to-Noise
Ratio with Lock-in Detection



Sep. 7th – Register now



Zurich
Instruments

Vibrational frequencies of CO bound to all three low-index cerium oxide surfaces: A consistent theoretical description of vacancy-induced changes using density functional theory

Cite as: J. Chem. Phys. 159, 034704 (2023); doi: 10.1063/5.0153745

Submitted: 11 April 2023 • Accepted: 19 June 2023 •

Published Online: 18 July 2023



View Online



Export Citation



CrossMark

Pablo G. Lustemberg,^{1,2,a)} Chengwu Yang,³ Yuemin Wang,⁴ Christof Wöll,^{4,b)} and M. Verónica Ganduglia-Pirovano^{2,b)}

AFFILIATIONS

¹Institute of Physics Rosario, IFIR, National Scientific and Technical Research Council, CONICET, and National University of Rosario, UNR, S2000EKF Rosario, Santa Fe, Argentina

²Institute of Catalysis and Petrochemistry, ICP, Spanish National Research Council, CSIC, 28049 Madrid, Spain

³School of Space and Environment, Beihang University, Beijing 100191, People's Republic of China

⁴Institute of Functional Interfaces, IFG, Karlsruhe Institute of Technology, KIT, 76344 Eggenstein-Leopoldshafen, Germany

^{a)}Present address: Physical Chemistry Department, Justus-Liebig-University Giessen, 35392 Giessen, Germany.

^{b)}Authors to whom correspondence should be addressed: christof.woell@kit.edu and vgp@icp.csic.es

ABSTRACT

The facet-dependent adsorption of CO on oxidized and reduced CeO₂ single crystal surfaces is reviewed, with emphasis on the effect of CO coverage and the ability of state-of-the-art quantum-mechanical methods to provide reliable energies and an accurate description of the IR vibrational frequency of CO. Comparison with detailed, high-resolution experimental infrared reflection absorption spectroscopy data obtained for single crystal samples allows the assignment of the different CO vibrational bands observed on all three low-index ceria surfaces. Good agreement is achieved with the hybrid density functional theory approach with the HSE06 functional and with saturation coverage. It is shown that CO is very sensitive to the structure of cerium oxide surfaces and to the presence of oxygen vacancies. The combined theoretical-experimental approach offers new opportunities for a better characterization of ceria nanoparticles and for unraveling changes occurring during reactions involving CO at higher pressures.

© 2023 Author(s). All article content, except where otherwise noted, is licensed under a Creative Commons Attribution (CC BY) license (<http://creativecommons.org/licenses/by/4.0/>). <https://doi.org/10.1063/5.0153745>

I. INTRODUCTION

Cerium dioxide (CeO₂ or ceria) is an important material in heterogeneous catalysis that has been used either as a catalyst or as a support material.¹ In addition, this rare-earth metal oxide has found applications in a number of other fields including solid-oxide fuel cells and even biology.^{2,3} Powder ceria materials, the most important form for technological applications, consist of nanometer- or micrometer-sized particles that expose facets with different crystallographic orientations. The different surfaces have rather different structures (see Fig. 1), and, as a result, exhibit different chemical activities. This fact has been concluded from several careful studies of chemical reactions carried out with ceria nanocrystals of

different morphologies, such as nanooctahedra (mostly exhibiting {111}-facets), nanocubes (mostly exhibiting {100}-facets), as well as nanorods (mostly exhibiting {110}- and {100}-facets).⁴⁻⁹

In order to rationalize the chemical activities of oxide powders in general and ceria nanoparticles in particular, reliable, easy-to-use methods are required to determine the nature of the exposed facets. In addition, it is important to note that the surfaces of the nanoparticles are not static; under reaction conditions (high pressure and elevated temperatures), the facets can undergo restructuring.¹⁰⁻¹⁴

When the particles are exposed to reducing conditions, this restructuring may include the creation of oxygen vacancies, the ease of which is strongly facet-dependent.¹⁵ Therefore, in order to get detailed insight into the mechanisms driving chemical reactions on

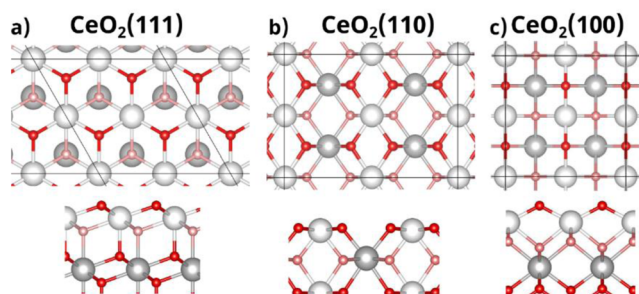


FIG. 1. Top and side views of the unrelaxed ceria surfaces: (a) (2×2) -(111), (b) (2×2) -(110), and (c) $p(2 \times 2)$ -(100) O-terminated with a calculated lattice constant of 5.398 Å (HSE06). Color code: Ce (O) atoms in the outermost layer are white (red), whereas those in deeper layers are gray (light red). This color code is used in all subsequent figures.

pure and metal-decorated ceria nanocrystals, it is mandatory to have available experimental methods capable of probing the surfaces of ceria-based catalysts under static and operando conditions with sufficient sensitivity to distinguish the different surface orientations and to provide information on the presence of oxygen vacancies. Among the existing experimental methods, the use of probe molecules like CO in connection with infrared (IR) vibrational spectroscopy, for example, in the surface-ligand IR (SLIR) approach,¹⁶ has been particularly successful. Carbon monoxide, or CO, is a popular probe molecule in the context of the SLIR approach. For numerous oxides [TiO₂ (anatase and rutile), Fe₂O₃, Fe₃O₄, ZnO, and CeO₂],¹⁷ it has been demonstrated that this probe molecule is very sensitive to the structure of oxide surfaces and can also be used to detect oxygen vacancies.^{18,19} In the case of ceria, numerous studies have been reported in the past for ceria powder samples exposed to CO.^{16,20–26}

However, there is no general consensus on the assignment of the different CO vibrational bands. For example, the band at about 2154 cm⁻¹ has been attributed to several different species such as physisorbed CO weakly bound to surface hydroxyl groups²² or CO adsorbed at under-coordinated Ce⁴⁺ ions in the vicinity of O vacancies.^{21,26} In view of these rather divergent assignments of experimental stretch frequencies, reliable reference data for CO adsorbed on model systems are required. Since even for well-defined model systems, i.e., single-crystal surfaces with low defect densities, ambiguities often exist in the assignment of vibrational features, a consistent theoretical description is also required. For example, even if there is only one possible adsorption site, different CO adsorbate species with varied tilt angles might exist (see below). In addition, it is important to know what the effect of oxygen vacancies is on the adsorbate frequencies. This information is a necessary condition for the characterization of the technologically relevant powder materials, which need to be characterized under reaction conditions. The interpretation of IR data acquired under operando conditions at higher pressures and elevated temperatures for ceria powders inside reaction chambers requires such reference data together with a reliable assignment obtained from *ab initio* density functional theory (DFT) calculations.

In the past, the application of theoretical methods, most of them employing density functional theory (DFT) with the generalized gradient approximation (GGA) for exchange and correlation,

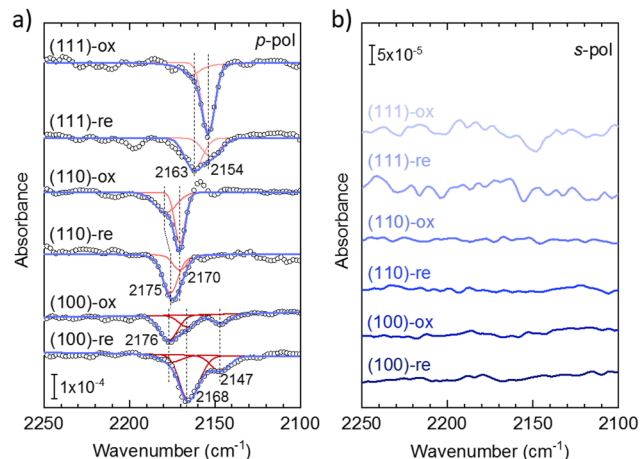


FIG. 2. Polarization-resolved IRRAS data of 1 ML CO adsorption on the oxidized and reduced (111), (110), and (100) ceria surfaces at 75 K: (a) p-polarized spectra; (b) s-polarized spectra.

has suffered from problems in accurately describing CO adsorbed on oxides.²⁷ In this case of rather weak adsorption, an accurate theoretical description of the CO binding as well as the CO vibrational frequencies represents a formidable challenge. These problems are in part due to the rather weak interaction of this small di-atomic molecule with oxide surfaces but also to inherent problems in describing the electronic structure of CO with DFT-GGA methods, e.g., the HOMO–LUMO gap of CO is $\sim 30\%$ small when using such a standard method.²⁸ In a recent paper,²⁹ we have demonstrated that in the case of the oxidized (111)- and (110)-surfaces of ceria, the DFT-GGA problems in accurately describing vibrational

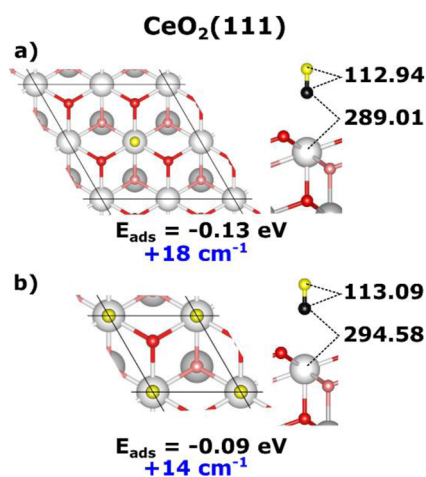


FIG. 3. Optimized structures of CO adsorption on the oxidized CeO₂(111) surface at CO coverages of (a) $\theta = 1/4$ and (b) $\theta = 1$, with (2×2) and (1×1) periodicity, respectively, and the HSE06 approach. The C and O atoms of the CO molecule are depicted in black and yellow, respectively. This color code is used in all subsequent figures. Selected distances (in pm) are indicated. The CO vibrational frequency shift ($\Delta\nu$ in cm⁻¹) is relative to the gas phase molecule.

TABLE I. Calculated literature values of the CO adsorption energy (E_{ads} in eV) and CO vibrational frequency shift ($\Delta\nu$ in cm^{-1}) relative to the gas phase molecule for CO bonding to the oxidized $\text{CeO}_2(111)$ surface at different CO coverages (in ML) with PBE+U and HSE06. For CO adsorption on the oxidized $\text{CeO}_2(111)$ surface, a blue shifted peak by $\Delta\nu = +11 \text{ cm}^{-1}$ is experimentally observed (cf. Fig. 2).

Oxidized $\text{CeO}_2(111)$						
References	Cell size	CO coverage	PBE+U		HSE06	
			$\Delta\nu$	E_{ads}	$\Delta\nu$	E_{ads}
Yang <i>et al.</i> ³¹	4×4	1/16	+2	-0.28
Yang <i>et al.</i> ¹²	4×4	1/16	+9	-0.28
Yang <i>et al.</i> ³³	3×3	1/9	+11	-0.29
Lustemberg <i>et al.</i> ²⁹	2×2	1/4	+2	-0.18	+18	-0.13
	1×1	1	+1	-0.03	+14	-0.09
	2×2^a	1	+0	-0.15	+13	-0.11

^aCorresponds to the concerted stretching mode of the four CO molecules. The other three collective modes have a negligible IR intensity (cf. Fig. S2).

frequencies of oxide-bound CO can be overcome by using a hybrid-DFT approach using mixtures of DFT(GGA) and Hartree-Fock exchange energies such as the HSE06 functional.³⁰ In the present paper, we demonstrate that with this approach, data for the reconstructed ceria (100)-surface as well as for the reduced (111), (110), and (100) surfaces can also be described and, furthermore, we now address the surface coverage effect on the calculated frequencies. The theoretical results are analyzed based on the comprehensive IRRAS (infrared reflection absorption spectroscopy) data of CO adsorbed on all three oxidized and reduced ceria single-crystal surfaces.^{12,31-33} In order to validate the importance of using the computationally rather expensive HSE06 functional to describe the CO-ceria interaction, we will, in all cases, compare the HSE06 results with those previously obtained using the standard PBE+U functional.

The paper is organized as follows. We will first discuss the theoretical results for the two nonpolar oxidized and reduced ceria (111) and (110) surfaces for two different CO coverages and compare them to the available experimental data. In the next step, we will consider the polar, reconstructed $\text{CeO}_2(100)$ surface, where the surface O atoms are removed in a checkerboard style, and demonstrate that with the HSE06 functional, a good agreement between experimental and theoretical data is also achieved for this surface. In addition, in this case, the presence of oxygen vacancies will be considered. We

will end by summarizing our findings and providing an outlook into the future.

II. MODELS AND METHODS

Spin-polarized DFT calculations were carried out using the slab-supercell approach³⁴ with the Vienna *Ab initio* Simulation Package (VASP, <http://www.vasp.at>; version 5.4.4).^{35,36} We treated the Ce (4f, 5s, 5p, 5d, 6s) and O (2s, 2p) electrons as valence states within the projector augmented wave (PAW) method with a plane-wave cutoff energy of 500 eV, whereas the remaining electrons were considered as part of the atomic cores. Strong correlation effects due to charge localization were considered by either adding a Hubbard U-like term³⁷ (referred to simply as U) for the Ce 4f states ($U = 4.5 \text{ eV}$)^{38,39} to the Perdew, Burke, and Ernzerhof (PBE) generalized gradient approximation (GGA) functional⁴⁰ or by using the hybrid-DFT HSE06 functional,^{30,41-45} which increases substantially the computational cost of plane-wave calculations. We note that dispersion forces are involved in adsorbate-surface interactions.^{46,47} In a previous study,²⁹ the effect of long-range dispersion corrections together with PBE+U and HSE06 was tested, and no significant effect was observed on either the calculated change in the C-O bond length upon adsorption or on the calculated frequency shift, $\Delta\nu$, although they did result in an increase in the bonding strength of CO to the ceria surface of $\approx 0.2 \text{ eV}$. Hence, in this work, dispersion corrections were not included in the calculations.

Bulk ceria has a cubic fluorite structure (*Fm3m*) with a calculated lattice constant of 5.485 Å (PBE+U) or 5.398 Å (HSE06). The low-index CeO_2 (111), (110), and (100) facets were modeled employing slab models with surface unit cells of two different sizes, namely, (1×1) and (2×2) , (1×1) and (2×2) , and (1×1) and $p(2 \times 2)$ periodicities, respectively (see Figs. 1 and S1), with the corresponding DFT-optimized lattice parameter; the number of layers used in each slab model is described in Table S1. The Monkhorst-Pack method⁴⁸ has been used to sample the Brillouin zones, and the k-meshes used for each structure are also included in Table S1. All supercells were set with a vacuum space of at least 15 Å.

TABLE II. Calculated HOMO-LUMO gap (in eV) for 1 ML bonded CO on top of a Ce^{4+} on all three oxidized low-index CeO_2 surfaces with PBE+U and HSE06 and (1×1) periodicity (cf. Figs. 3, 6, and 9). The difference between the methods (Δ) is also indicated.

Facet	Method	HOMO-LUMO gap	$\Delta(\text{HSE06-PBE+U})$
111	HSE06	9.21	1.33
	PBE+U	7.88	
110	HSE06	9.04	2.25
	PBE+U	6.79	
100	HSE06	5.04	2.56
	PBE+U	2.48	

The bulk-truncated oxygen-terminated (100) surface is polar, and thus surface reconstructions are expected. Different surface terminations with either Ce or O atoms in the outermost layer have been proposed in studies employing theoretical and experimental approaches.^{49–51} We here considered the *checkerboard* (100)–O termination (4O–4Ce–8O···4Ce–4O), in which 50% of the oxygen atoms in the bulk-truncated surface oxygen layer have been removed and placed at the bottom of the slab. This termination is 0.32 J/m² more stable than the corresponding (100)–Ce terminated one (2Ce–8O–4Ce···8O–2Ce).¹⁵ It should be mentioned that a mixture of O- and Ce-terminations can reduce the surface energy. For instance, the calculated surface energy for an 87.5%/12.5% [(100)–O]/(100)–Ce] mixed termination [$c(2 \times 2)$ unit cell] is by 0.03 J/m² smaller than that of the pure (100)–O termination, in agreement with what was observed by Pan *et al.*⁴⁹ We will not consider such mixed terminations of the (100) facet in more detail because it is beyond the scope of this work and only discuss the (100)–O, hereinafter referred to as (100).^{15,49–51}

All atoms in the bottom atomic layers were fixed, as indicated in Table S1, at their optimized bulk-truncated positions during geometry optimization, whereas the rest of the atoms were allowed to fully relax. Total energies and forces were calculated with a precision of 10^{–8} eV and 10^{–2} eV/Å for electronic and force convergence, respectively, for geometry optimization and the calculation of vibrational frequencies. When describing the outcome of the theoretical work and the experimental results, we will use the term “oxidized surface” to describe the results of the theoretical work carried out for a surface with an ideal CeO₂ stoichiometry. In the case of the experimental work, the term “oxidized surface” describes experimental results for a surface that has been oxidized using, for example, exposure to oxygen gas at elevated temperatures. In the latter case, however, a small concentration of oxygen vacancies cannot be excluded. The experimental preparation of a fully stoichiometric, ideal oxide surface is virtually impossible. The term “reduced surface” is used to describe the experimental results for a surface that has been reduced, for example, by annealing in ultra-high vacuum (UHV) conditions at high temperatures. There are a remarkable number of oxygen vacancies on the reduced surface.

The reduced surfaces were modeled by removing a surface oxygen atom from the slabs with the larger surface unit cell. The localization of the excess charge corresponds to that of the most stable structure, as previously reported.¹⁵ For the cases of the (111) and (100) surfaces, the presence of subsurface oxygen vacancies has also been considered.

The adsorption energy per CO molecule on the CeO₂ surfaces was calculated according to the following equation: $E_{ads} = (E[n \cdot \text{CO}/\text{CeO}_2] - E[\text{CeO}_2] - n \cdot E[\text{CO}_{gas}])/n$, where $E[\text{CO}/\text{CeO}_2]$ is the total energy of n CO molecules adsorbed on the surface, $E[\text{CeO}_2]$ is the total energy of the surface without the adsorbate, and $E[\text{CO}_{gas}]$ is the energy of the CO molecule in the gas phase.

The vibrational modes of adsorbed CO were calculated from a finite difference approximation of the dynamical matrix with 0.015 Å for the displacements as implemented in the VASP code, and the IR intensities from a finite difference approximation of the gradient of the z component of the dynamic dipole moment.⁵² Only the adsorbed CO was considered for the vibrational analysis. To simulate the vibrational spectrum, a summation of Gaussian

functions with a full width at half maximum (FWHM) of 10 cm^{–1} was employed.

CO in the gas phase was modeled using a single molecule in a cubic unit cell (8 × 8 × 8) Å³, sampled with the Γ -point. The computed CO stretching vibrational frequency for adsorbed CO on the ceria surfaces was scaled by the method-dependent factor $\lambda = \nu_{\text{CO}_{gas}}^{\text{exp}}/\nu_{\text{CO}_{gas}}^{\text{calc}}$ with $\nu_{\text{CO}_{gas}}^{\text{exp}} = 2143$ cm^{–1}¹⁵ and $\nu_{\text{CO}_{gas}}^{\text{calc}} = 2127$ and 2235 cm^{–1} for PBE+U and HSE06, respectively. The calculated C–O bond length of CO in the gas phase is 114.34 and 113.15 pm with PBE+U and HSE06, respectively.²⁶

III. RESULTS AND DISCUSSION

A. Experimental results

In Fig. 2, we summarize the results of polarization-resolved IRRAS experiments of 1 monolayer (ML) CO adsorbed on oxidized

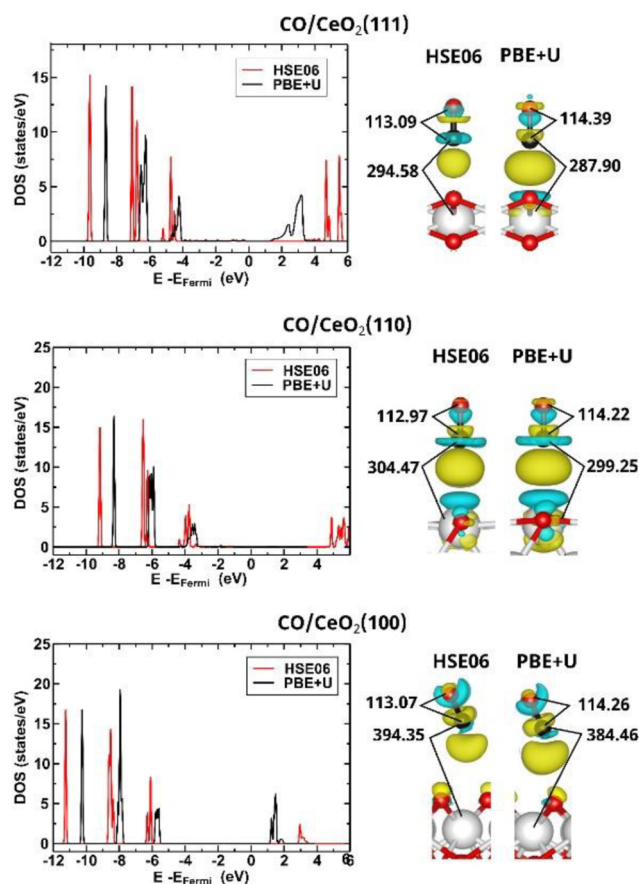


FIG. 4. Total density of states (DOS) projected onto the CO for 1 ML CO bound on top of a Ce⁴⁺ on all three oxidized low-index CeO₂ surfaces, the PBE+U and HSE06 approaches, and (1 × 1) periodicity and isosurfaces of the charge density difference, $\Delta\rho$, namely, that of the CO adsorbed system, from which both the charge density of the clean CeO₂ surface (with a structure corresponding to that of the adsorbed system) and that of the layer of adsorbed CO molecules have been subtracted [yellow (blue) corresponds to $\Delta\rho > 0$ (< 0)]. Selected interatomic distances (in pm) are indicated.

and reduced $\text{CeO}_2(111)$, (110), and (100) single-crystal surfaces at low temperatures (75 K) that have previously been published.^{12,31,33}

For the oxidized and reduced $\text{CeO}_2(111)$ surfaces that were prepared by repeated cycles of sputtering with 1 keV Ar^+ and annealing at 800 K for 15 min in an O_2 atmosphere of 1×10^{-5} mbar, or in UHV without O_2 to create the reduced one, a single intense CO band is visible for *p*-polarization at 2154 and 2163 cm^{-1} for the saturated surfaces, i.e., blue shifted by $\Delta\nu = +11$ and $+20 \text{ cm}^{-1}$ relative to the gas phase (2143 cm^{-1}), respectively.³¹ After similar treatments for the (110) surfaces, adsorbed CO shows a strong negative band at 2170 cm^{-1} , accompanied by a smaller positive feature at 2160 cm^{-1} for the oxidized surface and one band at 2175 cm^{-1} for the reduced one. Finally, CO adsorbed on the oxidized (100) surface reveals an intense band at 2176 cm^{-1} with a shoulder at 2168 cm^{-1} and a second weaker peak at 2147 cm^{-1} . Upon further reducing the surface by annealing to 800 K under UHV conditions, a shift of the main band from 2176 to 2168 cm^{-1} is observed, whereas the frequency of the low-lying band remains unchanged at 2147 cm^{-1} [Fig. 2(a)].

In the corresponding *s*-polarized IRRAS data [Fig. 2(b)], only a weak CO feature is resolved for the ceria (111) surface, while the CO vibrational signals are invisible for the (110) and (100) surfaces. These polarization-dependent IRRAS results reveal that all CO species adsorbed on the three oxidized and reduced ceria surfaces

adopt an upright or slightly tilted orientation, in line with the DFT calculations discussed below.

In Sec. III B, we will critically revise previous theoretical work and provided a consistent description of the experimental data.

B. Theoretical results

1. Oxidized (111) surface

Figure 3 shows the optimized structures and the calculated frequencies for adsorption of CO on the oxidized $\text{CeO}_2(111)$ surface at CO coverages of $\theta = 1/4$ and $\theta = 1$ ML with a (2×2) and (1×1) unit cell, respectively, and the HSE06 approach.²⁹ For the corresponding results with the PBE+U approach, see the supplementary material (Fig. S2). An adsorption site for CO atop Ce^{4+} is found, with the CO binding nearly perpendicular to the surface. At the (111) surface, there is only one type of Ce^{4+} ion exposed, which is 7-fold coordinated. At low CO coverage, the CO stretching frequency, ν , calculated with HSE06 shows a larger blue shift ($+18 \text{ cm}^{-1}$) than that calculated with the PBE+U approach ($+2 \text{ cm}^{-1}$). Similar results are obtained at full CO coverage with $\Delta\nu = +14$ and $+1 \text{ cm}^{-1}$ with HSE06 and PBE+U, respectively (Figs. 3 and S2). Furthermore, we note that the calculated adsorption energies become significantly lower with increasing CO coverage, from -0.18 eV for PBE+U and -0.13 eV

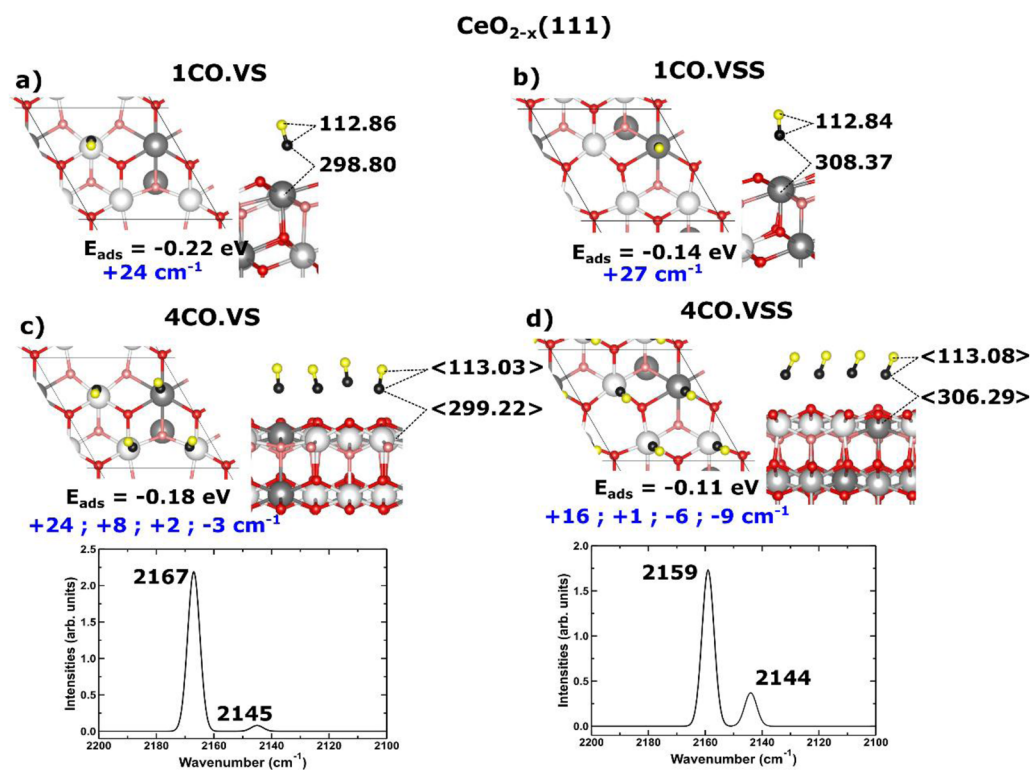


FIG. 5. Optimized structures of CO adsorption on the reduced $\text{CeO}_2(111)$ surface at CO coverages of (a) and (b) $\theta = 1/4$ (1 CO) and (c) and (d) $\theta = 1$ ML (4 CO) with (2×2) periodicity with either one surface (VS) or subsurface oxygen (VSS) vacancy in the outermost CeO_2 oxide layer and the HSE06 approach. Selected distances (in pm) are indicated; for the $\theta = 1$ case, distances correspond to averages. The CO vibrational frequency shift ($\Delta\nu$ in cm^{-1}) is relative to the gas phase molecule; for the $\theta = 1$ case, the shifts correspond to those of collective vibrational modes. Calculated IR spectra of 1 ML CO adsorption on reduced $\text{CeO}_2(111)$, for which a Gaussian broadening of 10 cm^{-1} has been used.

for HSE06 at $\theta = 1/4$ to -0.03 eV and -0.09 eV, respectively, at $\theta = 1$ (Fig. S2).

The calculated results with PBE+U and HSE06 for CO adsorption on the oxidized $\text{CeO}_2(111)$ surface are summarized in Table I and compared to previously published results.^{31–33} At this point, we note that in order to compare the calculated shifts with those observed experimentally, it is very important to consider the CO coverage. For example, it is tempting to interpret the experimental $\Delta\nu = +11$ cm^{-1} shift using the values calculated with PBE+U at considerably low coverages such as 1/16 and 1/9 ML, with $\Delta\nu = +9$ ³² and $+11$ ³³ cm^{-1} , respectively, but that is *not* correct. At CO saturation, the CO stretching vibrational frequency shift computed with the PBE+U approximation of about $+1$ cm^{-1} (Table I) is significantly smaller than the experimental value of $\Delta\nu = +11$ cm^{-1} (Fig. 2). However, the hybrid HSE06 functional predicts values of $\nu = 2156$ cm^{-1} and $\Delta\nu = +13$ cm^{-1} that are in good agreement with the experiment ($\nu = 2154$ cm^{-1} , Fig. 2).

Inspection of the structures for the adsorption of CO on the $\text{CeO}_2(111)$ surfaces (Figs. 4 and S2) reveals that the Ce–C distances are shorter with PBE+U than with HSE06. In addition, the C–O bond length is longer with PBE+U than with HSE06, and the corresponding changes in the C–O bond length, $\Delta d_{\text{C-O}}$, upon adsorption with respect to the calculated values for the gas phase molecule [114.34 (PBE+U) and 113.15 pm (HSE06)] show that (in most cases) $\Delta d_{\text{C-O}} > 0$ with PBE+U and $\Delta d_{\text{C-O}} < 0$ with HSE06. Specifically, the C–O bond is calculated to be compressed by 0.06 pm (expanded by 0.04 pm) when using the HSE06 (PBE+U) functional at saturation coverage (Fig. 4). The shorter the C–O bond, the higher the vibrational CO stretching frequency leading to a larger blue shift.

The overall change in the C–O bond upon adsorption is the result of synergistic charge transfer effects, namely, CO \rightarrow surface σ donation and surface \rightarrow CO π backdonation, which cause the shortening and lengthening of the C–O bond length, respectively. In a recent study,²⁹ we compared the density of states (DOS) for 1 ML of CO adsorbed on the oxidized $\text{CeO}_2(111)$ and (110) surfaces to that for the CO molecule in the gas phase. Figure 4 shows the DOS for 1 ML CO bound on top of a Ce^{4+} on all three oxidized low-index CeO_2 surfaces, clearly illustrating the differences in the electronic structure of the bonded CO, as described with PBE+U and HSE06; the HOMO–LUMO gap of CO is smaller when using the PBE+U method (cf. Table II). This occurs on all three low-index CeO_2 surfaces (cf. Table II). Moreover, compared to HSE06, the PBE+U approach predicts larger charge transfers, namely, CO \rightarrow surface, as evidenced by the more pronounced electron density accumulation in the shorter Ce–C bond, and surface \rightarrow CO, as evidenced by the enhancement electron density at the O end of the longer C–O bond, and as a result, $\Delta d_{\text{C-O}} > 0$ (Fig. 4).

2. Reduced (111) surface

The reduced CeO_{2-x} (111) surface has been extensively studied (see Ref. 15 and references therein). The most recent studies in the literature, independently of the specific implementation of periodic DFT calculations (different unit cell sizes, underlying exchange–correlation functional, U value in DFT+U, etc.), generally agree that the subsurface vacancy (VSS) is more stable than the superficial one (VS) and that the Ce^{3+} ions prefer sites that are not adjacent to the vacancies, preferably in the outermost cationic layer (cf. Fig. S1). In the case of a reduced surface with (2×2) periodicity, the subsurface

vacancy is more stable than the surface vacancy by ~ 0.4 eV (PBE+U), with the Ce^{3+} in the next-nearest neighboring cation sites to the vacant oxygen site for both types of vacancies, one in the outermost cationic plane and the other in the plane below.

Figure 5 shows the optimized structures and the calculated frequency shifts for CO adsorption on the reduced $\text{CeO}_{2-x}(111)$ surface with (2×2) periodicity (1 CO, $\theta = 1/4$) with either one surface of subsurface oxygen vacancy in the outermost CeO_2 oxide layer or the HSE06 approach. For the corresponding results with the PBE+U approach, see the supplementary material (Fig. S3, Table S2). The CO species on top of the nearest neighbor surface Ce^{4+} cation to the surface oxygen vacancy is more stable than that on top of the next-nearest neighbor surface Ce^{3+} cation (not shown). With HSE06, the latter structure is, in fact, unstable, and with the PBE+U approach, it is ~ 0.1 eV less stable than on top of a Ce^{4+} , a configuration for which the calculated adsorption energies are comparable (Fig. S3, Table S2), cf. -0.22 (HSE06) to -0.24 eV (PBE+U). However, the calculated frequency shift with HSE06 ($+24$ cm^{-1}) is much larger than that with PBE+U ($+3$ cm^{-1}). In the case of a subsurface oxygen vacancy, the CO species on top of the next-nearest neighbor surface Ce^{3+} cation is less than ~ 0.05 eV more stable than that on top of the nearest neighbor surface Ce^{4+} cation (not shown) with both approaches, and the calculated adsorption

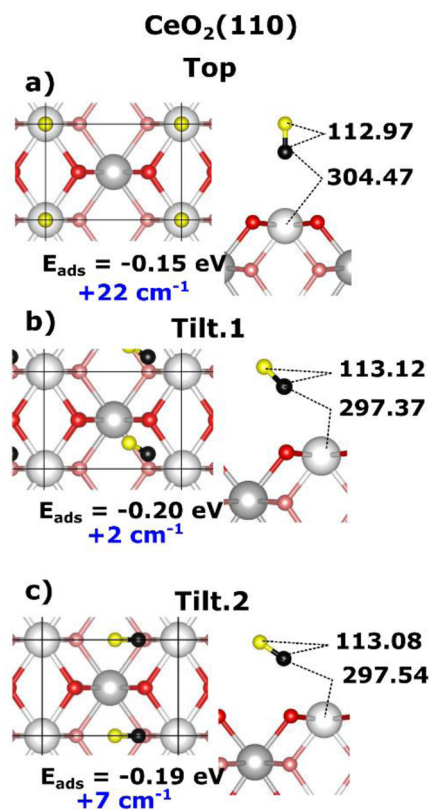


FIG. 6. Optimized (a) top and (b) and (c) tilted structures of CO adsorption on the reduced $\text{CeO}_2(110)$ surface at $\theta = 1$ ML CO coverage with (1×1) periodicity and the HSE06 approach. Selected distances (in pm) are indicated. The CO vibrational frequency shift ($\Delta\nu$ in cm^{-1}) is relative to the gas phase molecule.

energies are comparable (Fig. S3, Table S2), cf. -0.14 (HSE06) and -0.18 eV (PBE+U). In addition, in this case, the calculated frequency shift with HSE06 ($+27$ cm^{-1}) is larger than that with PBE+U ($+17$ cm^{-1}).

For a higher CO coverage of $\theta = 1$ (Figs. 5 and S3, Table S2), with 4 CO molecules, each of them on top of a surface cationic site ($3 \times \text{Ce}^{4+}$ and $1 \times \text{Ce}^{3+}$), the calculated adsorption energies for both surface and subsurface vacancy types, and with both computational approaches, are slightly lower compared to those at the lower CO coverage of $\theta = 1/4$ (cf. -0.19 to -0.24 eV with PBE+U and -0.18 to -0.22 eV with HSE06 for the example of the surface vacancy). However, similarly to the case of $\theta = 1/4$, the frequency shifts are significantly influenced by the computational approach (cf. Figs. 5 and S3, Table S2).

Two factors need to be considered when comparing the calculated shifts with the experimental one of $+20$ cm^{-1} (cf. Fig. 2), namely, the approximation to exchange and correlation and the CO coverage. For instance, at $1/4$ ML, PBE+U with shifts of $+3$ and $+17$ cm^{-1} for surface and subsurface vacancies, respectively (Fig. S3, Table S2), would erroneously suggest that CO could be used to probe the subsurface nature of the vacant sites,^{31,32} but that is not true as explained below. Moreover, upon increasing the CO coverage from $1/4$ to 1 ML with PBE+U, the shift in the presence of a subsurface oxygen vacancy decreases dramatically from $+17$ cm^{-1} for CO coverage of $\theta = 1/4$ to $+2$ cm^{-1} for $\theta = 1$ (Fig. S3, Table S2). However, HSE06, with a corresponding shift of $+16$ cm^{-1} at 1 ML (Fig. 5), provides a much better agreement with the experiment [$+20$ cm^{-1} , cf.

Figs. 5(c), 5(d), and 2]. Nonetheless, given the similarities of the values of $\Delta\nu$ calculated for the cases of surface and subsurface vacancies (Fig. 5), CO would not allow unequivocally characterizing the nature of the oxygen vacancies near the surface, but O_2 does.³²

3. Oxidized (110) surface

For CO adsorption on the $\text{CeO}_2(110)$ surface, two blue shifted peaks by $\Delta\nu = +27$ and $+11$ cm^{-1} are experimentally observed (Fig. 2). The structure of (110) facets is shown in Fig. 1. The surface exposes Ce^{4+} cations coordinated to six oxygen atoms, two in the top plane and four in the plane below. Figure 6 shows the optimized structures and the calculated frequency shifts for the adsorption of CO on the oxidized $\text{CeO}_2(110)$ surface at 1 ML CO coverage with a (1×1) unit cell and the HSE06 approach.²⁹ For the corresponding results with the PBE+U approach, see the supplementary material (Fig. S4, Table S3). An adsorption site for CO atop Ce^{4+} is found, with the CO binding nearly perpendicular to the surface. Interestingly, the calculations revealed that in addition to this upright adsorption geometry, two tilted configurations with slightly larger binding energies (by ~ 0.05 eV) were also found (Fig. 6). The difference between the tilted configurations is that in one case, the CO molecule points to the Ce^{4+} cation in the second oxide plane (Tilt.1, Fig. 6), and in the other one, to the Ce^{4+} cation on the surface (Tilt.2, Fig. 6).

The PBE+U calculated binding energy for the atop Ce^{4+} site $\lesssim 0.2$ eV (in absolute value, Fig. S4, Table S3) is consistent with that

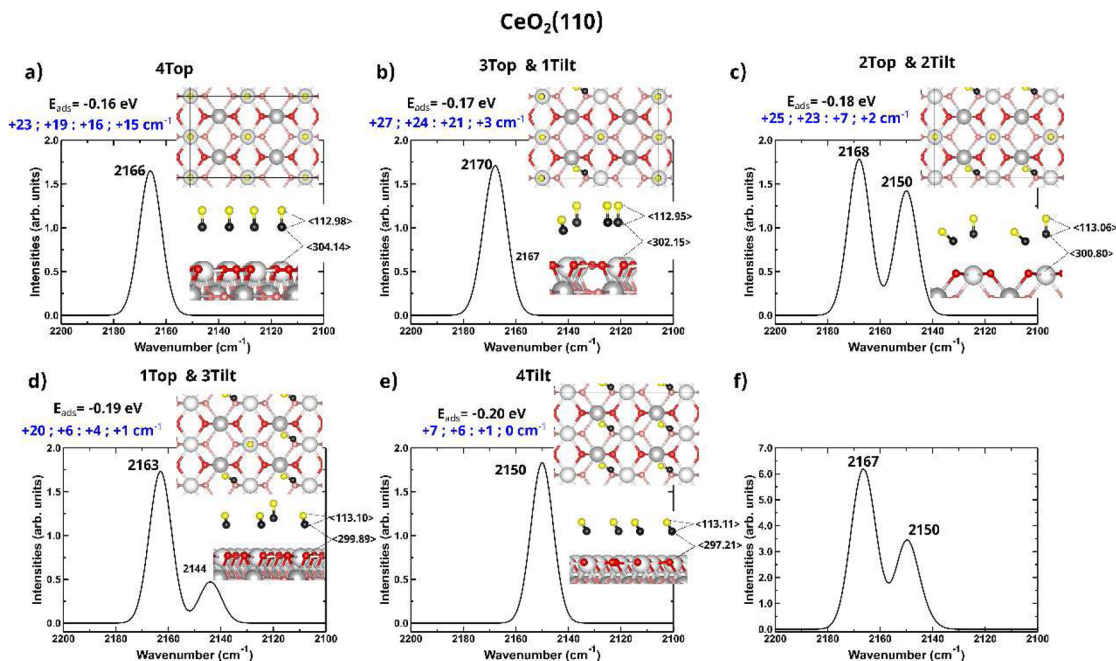


FIG. 7. (a)–(e) Optimized structures and intensities of IR-active bands for adsorption of CO on the oxidized $\text{CeO}_2(110)$ surface at CO coverage of $\theta = 1$ with a (2×2) unit cell and the HSE06 approach. Selected average distances (in pm) are indicated. The CO vibrational frequency shift ($\Delta\nu$ in cm^{-1}) is relative to the gas phase molecule; the shifts correspond to those of collective vibrational modes. Calculated IR spectra of 1 ML CO adsorption on reduced $\text{CeO}_2(111)$, for which a Gaussian broadening of 10 cm^{-1} has been used. The last spectrum (f) corresponds to the sum of all the spectra corresponding to the five different configurations considered.

of previous PBE/PW91 + $U(4.5/5)$ [-0.19^{53} and -0.21^{54} eV with (2×2) unit cells] and PBE/PW91 [-0.16^{53} and -0.18^{55} eV with (2×2) and (1×2) unit cells, respectively] studies. The HSE06 calculated binding energies are comparable to those obtained with PBE+ U (Fig. S4, Table S3).

Only the HSE06 calculated CO stretching frequencies, ν , and their shifts with respect to those of the free molecule, $\Delta\nu$, are in good agreement with the results of the IRRAS experiment, with deviations <9 cm^{-1} . The more intense band at 2170 cm^{-1} and the less intense one at 2154 cm^{-1} observed with p -polarized light are assigned to CO bound to Ce^{4+} in atop and slightly tilted configurations, respectively (cf. Figs. 2 and 6). While the agreement with the HSE06 calculations is rather good, the deviations of the computed ν and $\Delta\nu$ values for CO adsorbed on the $\text{CeO}_2(110)$ surface with PBE+ U from the experimental ones are substantial. In particular, for the tilted configuration, a red shift of $\Delta\nu = -23$ cm^{-1} is computed, clearly outside the experimental error (Fig. S4, Table S3). Herschend *et al.*⁵⁶ reported a blue-shifted peak of $+9$ cm^{-1} for the top configuration obtained using hybrid-DFT embedded cluster calculations, but a red shift of -5 cm^{-1} and a smaller bandgap with a GGA functional (cf. Table II).

As in the case of the (111) orientation discussed earlier, the geometric and electronic structures for the adsorption of CO on the $\text{CeO}_2(110)$ surfaces were inspected. Figure S4 reveals that the Ce–C distances are shorter with PBE+ U than with HSE06. In addition, the C–O bond length is longer with PBE+ U than with HSE06, and the corresponding changes in the C–O bond length, $\Delta d_{\text{C-O}}$, upon adsorption with respect to the calculated values for the gas phase molecule [114.34 (PBE+ U) and 113.15 pm (HSE06)] show that (in most cases) $\Delta d_{\text{C-O}} > 0$ with PBE+ U and $\Delta d_{\text{C-O}} < 0$ with HSE06. Specifically, the C–O bond is calculated to be compressed by 0.18 pm and up to about 0.1 pm in the atop and tilted configurations, respectively, when using the HSE06 functional at saturation coverage. A compression of about 0.1 pm has been previously calculated for the atop configuration employing the hybrid B3LYP functional.⁵⁷ However, for the tilted configurations, the PBE+ U calculated C–O bond is stretched by about 0.1 pm in both cases. As for the electronic structure, for all configurations, the HOMO–LUMO gap of CO is smaller, and the CO \rightarrow surface and surface \rightarrow CO charge transfers are larger with PBE+ U than with HSE06 (cf. Table II and Fig. 4 for the example of the top configuration at saturation coverage).

The coupling between adjacent CO molecules on $\text{CeO}_2(110)$ is rather weak. To demonstrate that we have performed additional calculations for differently ordered phases of CO on the $\text{CeO}_2(110)$ surface with (2×2) periodicity and 1 ML with HSE06 (Fig. 7). Five different arrangements for the four CO molecules have been explored, including configurations with $4 \times$ Tilt.1, $3 \times$ Tilt.1 and $1 \times$ Top, $2 \times$ Tilt.1 and $2 \times$ Top, $1 \times$ Tilt.1 and $3 \times$ Top, and $4 \times$ Top CO. The calculated vibrational frequencies indicate that the in-phase collective stretching of all four CO tilted molecules and that of all four atop molecules are hardly affected when the mixed structure is considered.²⁹ In these cases, the concerted in-phase stretching mode of the four CO molecules is the one that has a non-negligible IR intensity, while the other three collective modes do (Fig. 7).

For the adsorption of $1/4$ ML CO on to the oxidized (110) surface with (2×2) periodicity, a similar performance of the PBE+ U and HSE06 approaches for the description of the interaction of the surface bound CO has been found, compared to the results for 1 ML (Fig. S4, Table S3).²⁹ As for the (111) surfaces discussed earlier, the

results at saturation coverage with the HSE06 functional provide the best agreement with the experimental values.

4. Reduced (110) surface

The reduced CeO_{2-x} (110) surface has also been studied (see Ref. 15 and references therein). The surface vacancy is more stable than the subsurface vacancy by ~ 0.9 eV [PBE+ U with (2×2) periodicity], with both Ce^{3+} cations in the first ceria layer, one in the nearest neighbor position and the other in the next-nearest neighbor position (cf. Fig. S1). For CO adsorption on the reduced $\text{CeO}_2(110)$ surface, a blue shifted peak by $\Delta\nu = +32$ cm^{-1} is experimentally observed (Fig. 2).

Figure 8 shows the optimized structures and the calculated frequency shifts for CO adsorption on the reduced $\text{CeO}_{2-x}(110)$ surface at CO coverages of $\theta = 1/4$ (1 CO) and $\theta = 1$ ML (4 CO) with (2×2) periodicity, with one surface oxygen vacancy (VS), and the HSE06 approach. For the corresponding results with the PBE+ U approach, see the supplementary material (Fig. S5, Table S4). At $\theta = 1/4$, CO species bind on top of a nearest neighbor surface Ce^{4+} cation to the surface oxygen vacancy with both HSE06 and PBE+ U approaches. However, the calculated frequency shift with HSE06 ($+22$ cm^{-1}) is significantly different from that with PBE+ U (-32 cm^{-1}).

For the higher CO coverage of $\theta = 1$ (Figs. 8 and S5, Table S4), with 4 CO molecules, each of them on top of a surface cationic

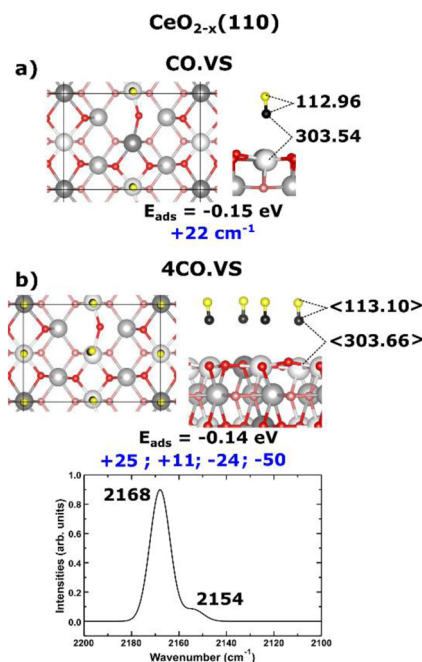


FIG. 8. Optimized structures of CO adsorption on the reduced $\text{CeO}_2(110)$ surface at CO coverages of (a) $\theta = 1/4$ (1 CO) and (b) $\theta = 1$ ML (4 CO) with (2×2) periodicity with one surface (VS) oxygen vacancy in the outermost CeO_2 oxide layer and the HSE06 approach. Selected distances (in pm) are indicated; for the $\theta = 1$ case, distances correspond to averages. The CO vibrational frequency shift ($\Delta\nu$ in cm^{-1}) is relative to the gas phase molecule; for the $\theta = 1$ case, the shifts correspond to those of collective vibrational modes. Calculated IR spectra of 1 ML CO adsorption on reduced $\text{CeO}_2(110)$, for which a Gaussian broadening of 10 cm^{-1} has been used.

site ($3 \times \text{Ce}^{4+}$ and $1 \times \text{Ce}^{3+}$; upon CO adsorption, one of the excess electrons, initially at the surface, moved to a deeper oxide layer), the calculated adsorption energy is slightly lower compared to that at the lower CO coverage of $\theta = 1/4$ with both computational approaches (cf. -0.17 to -0.21 eV with PBE+U and -0.14 to -0.15 eV with HSE06, Table S4). However, similarly to the case of $\theta = 1/4$, the frequency shifts are significantly influenced by the computational approach (Fig. S5). CO adsorption at saturation coverage on the reduced CeO_{2-x} (110) surface shows a blue shifted peak by $+25 \text{ cm}^{-1}$ with HSE06, providing a much better agreement with the experiment than PBE+U [cf. Figs. 8(b) and 2].

5. Oxidized (100) surface

As mentioned earlier, we here consider the checkerboard O-terminated surface (Fig. 1). For CO adsorption on the CeO_2 (100) surface, an intense blue-shifted peak by $\Delta\nu = +33 \text{ cm}^{-1}$ with a shoulder at 2168 cm^{-1} ($\Delta\nu = +25 \text{ cm}^{-1}$) and a second weaker peak shifted by $+4 \text{ cm}^{-1}$ are experimentally observed (Fig. 2). Figure 9 shows the stable structures and the calculated frequencies for adsorption of CO on the oxidized CeO_2 (100) surface at the saturation CO coverage of $\theta = 1$ with a (1×1) unit cell and the HSE06 approach. For the corresponding results with the PBE+U approach, see the supplementary material (Fig. S6, Table S5). Two adsorption sites were found with CO binding nearly perpendicular to the surface, namely, CO on top of the Ce^{4+} cations and in a $\text{Ce}^{4+}-\text{Ce}^{4+}$ bridge configuration with a significantly larger binding energy (Fig. 9). As for the (111) and (110) surfaces (cf. Figs. 3 and 6), inspection of the structures for the adsorption of 1 ML CO on the CeO_2 (100) surfaces (Fig. S6) reveals that the Ce–C distance and the C–O bond length are shorter and longer, respectively, with PBE+U than with HSE06. In line with the calculated structures, the CO stretching frequencies calculated with HSE06 show a larger blue shift, $+33$ and $+8 \text{ cm}^{-1}$, for the bridge and top configurations, respectively, than those calculated with the PBE+U approach, $+9$ and $+6 \text{ cm}^{-1}$, respectively (Fig. S6, Table S5). A similar result is obtained for the most stable bridge site at the lower CO coverage of $\theta = 1/4$ with a (2×2) unit cell with $\Delta\nu = +41$ and $+15 \text{ cm}^{-1}$ with HSE06 and PBE+U, respectively (Fig. S6, Table S5). We note that the calculated adsorption energies become lower with increasing CO coverage, from -0.41 eV at $\theta = 1/4$ to -0.29 eV at $\theta = 1$ for the bridge site with HSE06 (Fig. 9).

It is clear that the frequency shifts calculated with HSE06 at saturation coverage for CO species at the bridge and atop sites, $+33$ and $+8 \text{ cm}^{-1}$, respectively, agree very well with the experimental results of $+33$ and $+4 \text{ cm}^{-1}$, respectively (cf. Fig. 2). The shoulder at $+25 \text{ cm}^{-1}$ is related to the presence of surface oxygen vacancies, as discussed in Sec. III B 6. Once again, we stress here the importance of considering not only the exchange-correlation functional used but also the CO coverage when comparing the calculated values of the frequency shifts with the measured ones for both the oxidized and reduced surfaces (cf. Sec. III B 6). We note that in the literature,³³ based on calculated vibrational frequencies with PBE+U and a $c(2 \times 2)$ unit cell with one surface oxygen vacancy and a CO coverage of $\theta = 1/9$ (Table S6), the signal shifted by $+4 \text{ cm}^{-1}$ has been wrongly assigned to CO adsorbed to bridge sites at ideal patches of the surface or at some distance from surface oxygen vacancies, whereas the signal shifted by $+33 \text{ cm}^{-1}$ and the shoulder at $+25 \text{ cm}^{-1}$ have also been wrongly assigned to CO bound at a surface oxygen vacant site with two nearest-neighbor Ce^{3+} and Ce^{4+} , respectively.

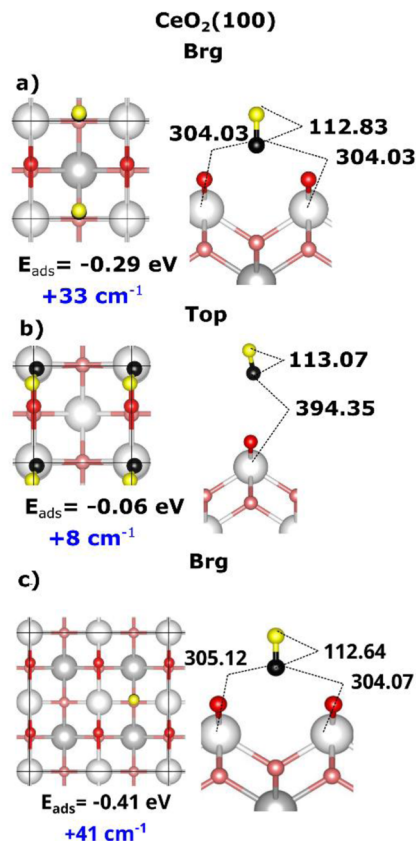


FIG. 9. Optimized structures of CO adsorption on the oxidized CeO_2 (100) surface at CO coverages of (a) and (b) $\theta = 1$ and (c) $\theta = 1/4$, with (1×1) and (2×2) periodicity, respectively, and the HSE06 approach. Selected distances (in pm) are indicated. The CO vibrational frequency shift ($\Delta\nu$ in cm^{-1}) is relative to the gas phase molecule.

6. Reduced (100) surface

The reduced CeO_{2-x} (100) surface has also been investigated (see Ref. 15 and references therein). In the case of the reduced surface with one oxygen vacancy with a $p(2 \times 2)$ periodicity, the stability of surface and subsurface vacancies is comparable (within ~ 30 meV, PBE+U), with one Ce^{3+} in the outermost cationic plane and the other one in the plane below for both types of vacancies. In the case of the surface vacancy, one Ce^{3+} is in the nearest and the other in the next-nearest neighboring cation site to the vacancy, whereas for the subsurface vacancy, they are both next-nearest neighbors (cf. Fig. S1). For CO adsorption on the reduced CeO_2 (100) surface, an intense blue-shifted peak by $\Delta\nu = +25 \text{ cm}^{-1}$ with two shoulders at $\Delta\nu = +33$ and $+4 \text{ cm}^{-1}$ is experimentally observed (Fig. 2). The two shoulders correspond to the two peaks observed for the oxidized surface discussed earlier.

Figure 10 shows the optimized structures and the calculated frequency shifts for CO adsorption on the reduced CeO_{2-x} (100) surface with a surface or subsurface vacancy at the saturation CO coverage of $\theta = 1$ ML (4 CO), with $p(2 \times 2)$ periodicity and the HSE06 approach. For the corresponding results with the PBE+U approach,

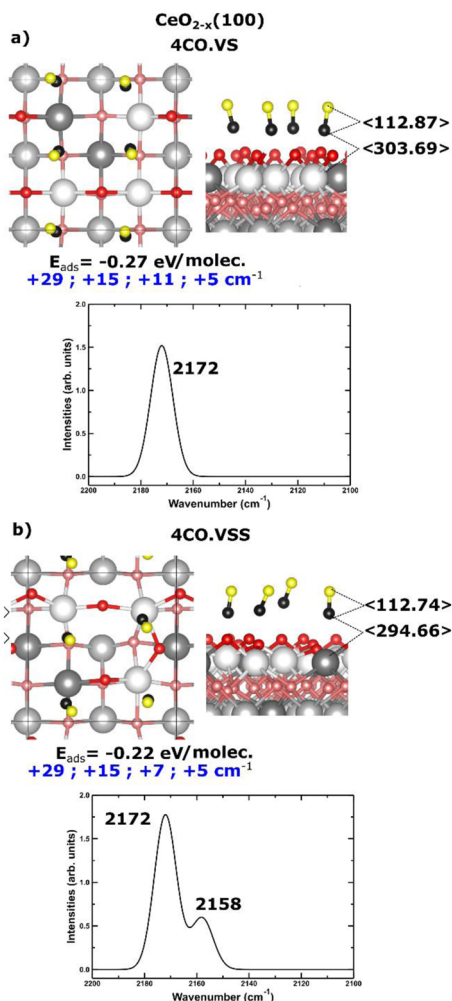


FIG. 10. Optimized structures for adsorption of CO on the reduced $\text{CeO}_{2-x}(100)$ surface with one (a) surface (VS) or (b) subsurface (VSS) oxygen vacancy in the outermost CeO_2 oxide layer at CO coverage of $\theta = 1$ with a (2×2) unit cell and the HSE06 approach. Selected average distances (in pm) are indicated. The CO vibrational frequency shift ($\Delta\nu$ in cm^{-1}) is relative to the gas phase molecule; the shifts correspond to those of collective vibrational modes. Calculated IR spectra of 1 ML CO adsorption on reduced $\text{CeO}_2(100)$, for which a Gaussian broadening of 10 cm^{-1} has been used.

see the supplementary material (Table S7). The calculated largest frequency shifts with HSE06 ($+29 \text{ cm}^{-1}$) for both types of vacancies are significantly different from those with PBE+U ($+14$ and $+12 \text{ cm}^{-1}$ for the surface and subsurface vacancies, respectively). Similar to the $\text{CeO}_2(100)$ surface, the frequencies calculated with HSE06 for CO species at oxygen vacancy sites correspond well to an intense blue-shifted peak by $\Delta\nu = +25 \text{ cm}^{-1}$ (Fig. 2). For both HSE06 and PBE+U, CO does not distinguish between surface and subsurface vacancies.

As mentioned earlier, the signal shifted by $+25 \text{ cm}^{-1}$ has earlier been wrongly assigned to CO bound at a surface oxygen vacancy

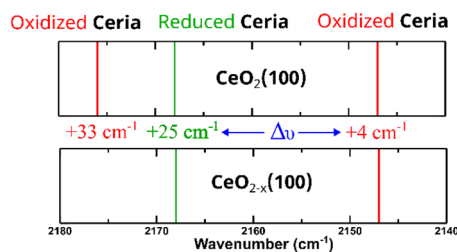


FIG. 11. Assignment of the observed IR spectra of CO adsorption on the oxidized and reduced $\text{CeO}_2(100)$ surface (Fig. 2) based on calculations with HSE06 at the saturation coverage of 1 ML.

site with two nearest-neighbor Ce^{4+} , based on vibrational frequencies with PBE+U and a $c(2 \times 2)$ unit cell with one surface oxygen vacancy and a CO coverage of $\theta = 1/9$ (cf. Fig. S8).³³ We have not only repeated those calculations (Table S6) but also considered the cases of CO adsorption on the reduced $\text{CeO}_{2-x}(100)$ surface at a CO coverage of $\theta = 1/4$ with $p(2 \times 2)$ periodicity, with one surface or subsurface oxygen vacancy, and the PBE+U approach. At $\theta = 1/4$, a large number of configurations have similar adsorption energies (Fig. S7). For example, for two of the stable sites in the bridge oxygen vacancy case, in which CO species bind in a bridge configuration with subsurface oxygen below, a frequency shift of $+30$ and $+17 \text{ cm}^{-1}$ was calculated for a $\text{Ce}^{4+}-\text{Ce}^{4+}$ and a $\text{Ce}^{3+}-\text{Ce}^{4+}$ bridge, respectively. However, when CO occupies all Ce-bridge sites at saturation coverage ($\theta = 1$), the frequency shift of the collective in-phase stretch vibration is $+14 \text{ cm}^{-1}$ (Fig. 10). These results show once again the significant effect that CO coverage could have on the calculated frequencies.

Figure 11 shows the assignments of the experimentally observed shifts (Fig. 2) for CO adsorption on the oxidized and reduced (100) surfaces at saturation CO coverage based on HSE06 calculations (cf. Figs. 9 and 10).

We note that the band shifted by $+4 \text{ cm}^{-1}$ is observed for both reduced and oxidized surfaces with similar intensity (Fig. 2). The intensity and sign of vibrational bands in IRRAS can vary strongly depending on the interaction of the transition dipole moment with the p- and s-polarized components of the incident light. For the reduced $\text{CeO}_2(100)$ surface, the intensity of the 2147 cm^{-1} band could be explained in terms of the slight modification of the chemical environment of this CO species on the reduced surface. Based on our HSE06 data in Figs. 9 and 10, it is attributed to CO at atop Ce^{4+} sites rather than to an O-vacancy related CO species.

IV. CONCLUSIONS

The vibrational frequencies of CO bound to all three oxidized and reduced low-index cerium oxide surfaces have been theoretically investigated and compared with the experimental results of a state-of-the-art high-resolution IR spectroscopy study performed on single crystal samples.²⁹ The theoretical results for the oxidized (111) and (110) facets at full CO coverage (1 ML) are independent of the cell size used (1×1 or 2×2 with one or four CO molecules, respectively). Importantly, only the computational results obtained with the HSE06 functional are in good agreement with the experiment and reproduce the experimentally observed blue frequency shifts

TABLE III. Data for the adsorption of 1 ML CO on the three low-index oxidized and reduced CeO₂ surfaces. The CO adsorption site, the localization of the oxygen vacancy [surface (VS)/subsurface vacancy (VSS)], the adsorption energy (E_{ads} in eV), and the vibrational frequency shift ($\Delta\nu$ in cm⁻¹) are indicated.

Method	CO site	E_{ads} (eV)	ν (cm ⁻¹)	Method	Vacancy site	E_{ads} (eV)	ν (cm ⁻¹)
CO/CeO ₂ (111) (1 × 1)				CO/CeO _{2-x} (111) (2 × 2)			
IRRAS			2154	IRRAS			2163
HSE06 (PBE+U)	Top	-0.09 (-0.03)	2157 (2144)	HSE06 (PBE+U)	VS/VSS	-0.18/-0.11 (-0.19/-0.13)	2167/2159 (2145/2145)
CO/CeO ₂ (110) (1 × 1)				CO/CeO _{2-x} (110) (2 × 2)			
IRRAS			2170/2160	IRRAS			2175
HSE06 (PBE+U)	Top Tilt.1 Tilt.2	-0.15 (-0.16) -0.20 (-0.22) -0.19 (-0.21)	2165 (2151) 2145 (2120) 2150 (2130)	HSE06 (PBE+U)	VS	-0.14 (-0.17)	2168 (2146)
CO/CeO ₂ (100) (1 × 1)				CO/CeO _{2-x} (100) (2 × 2)			
IRRAS			2176/2168/2147	IRRAS			2168/2147
HSE06 (PBE+U)	Bridge Top	-0.29 (-0.31) -0.06 (-0.04)	2176 (2152) 2151 (2149)	HSE06 (PBE+U)	VS VSS	-0.27 (-0.32) -0.22 (-0.23)	2172 (2157) 2172 (2155)

(Table III). In both cases, a nearly perpendicular top Ce⁴⁺ adsorption site has been found, and on the (110) facet, two tilted configurations have also been found. The calculated blue shifts of $\Delta\nu = +1, +8$ cm⁻¹ with PBE+U for a top configuration on the (111) and (110) facets at full coverage, respectively, and red shifts of -23 and -13 cm⁻¹ for the tilted configurations on the (110), substantially deviate from the experimental values of $\Delta\nu = +11$ cm⁻¹ for both top configurations and $+27$ cm⁻¹ for the tilted ones. Moreover, it is observed that by decreasing the CO coverage from 1 to 1/4 ML, larger shifts are generally obtained with both computational approaches and for both oxidized and reduced surfaces. For example, for the top configurations, shifts of $\Delta\nu = +2, +11$ cm⁻¹ on the oxidized (111) and (110) facets, respectively, have been obtained with PBE+U and 1/4 ML CO coverage, i.e., an increase of $+1$ and $+3$ cm⁻¹, respectively, compared to 1 ML. The corresponding increases with HSE06 are $+4$ and $+1$ cm⁻¹.

For the reduced CeO_{2-x}(111) surface at full CO coverage, it is difficult to discern whether the experimental shift of $+20$ cm⁻¹ is due to the presence of a surface or subsurface vacancy since, with HSE06, shifts of $+24$ and $+16$ cm⁻¹, respectively, have been obtained (Table III). The corresponding values with PBE+U are $+2$ cm⁻¹ for both cases, which are clearly not in agreement with the experimental value of $+20$ cm⁻¹. The reduced CeO_{2-x}(111) surface is another example of how important it is to consider both the actual experimental CO coverage in the model and the accuracy of the approximation to exchange and correlation in the DFT calculations. For example, shifts of $+3$ and $+17$ cm⁻¹ due to the presence of a surface or subsurface vacancy have been obtained with PBE+U and 1/4 ML CO coverage, mistakenly suggesting that CO would

distinguish the nature of oxygen vacancies. Furthermore, for the reduced CeO_{2-x}(110) surface at full CO coverage, only the presence of surface vacancies has been considered, and at full CO coverage, a shift of $+25$ cm⁻¹ has been obtained with HSE06, in good agreement with the experimental value of $+32$ cm⁻¹, while the corresponding PBE+U result is $+3$ cm⁻¹.

For the CeO₂(100) surface, we provide a new CO band assignment as a result of having considered full CO coverage and the HSE06 functional (Table III). Our results with HSE06 indicate that the experimentally observed blue shifts of $+33$ and $+4$ cm⁻¹ correspond to the adsorption of CO on the bridge and top sites of the oxidized (100) surface, whereas the shift of $+25$ cm⁻¹ corresponds to the adsorption of CO on the reduced surface. In this case, it is also difficult to discern whether the experimental shift of $+25$ cm⁻¹ is due to the presence of a surface or subsurface vacancy.

The HSE06 method is computationally very expensive compared to PBE+U. On average, the computational time, calculated as [Number of central processing units (CPUs)] × (time), of a structure relaxation with HSE06 is $100\times$ more expensive than with PBE+U. As an example, 384 CPU hours (96 CPUs × 4 h) were required for the structure optimization of CO/CeO₂(111) with 1×1 periodicity with the HSE06 method. However, the choice of the model (CO coverage) and the methodology are crucial to obtain a more accurate description of the geometric and electronic structures of the CO/CeO₂ systems and, in turn, of the CO vibrational spectra. The HSE06 method does cure the shortcomings of the PBE+U, such as the small HOMO-LUMO gap of CO and the large CO→surface and surface→CO charge transfers.

The experimental know-how in the field is growing, but it is only recently that detailed high-resolution IR spectroscopy studies on CO adsorption on single crystal oxide sample surfaces can be performed.^{16,17} Joint efforts are likely to improve our knowledge of the CO vibrational bands observed on differently oriented surfaces and the defect-induced changes. Considering our results for the CO/CeO₂ systems, we think that there is room for surprises if other CO/oxide systems are revisited. Our findings thus provide a theoretical basis for the detailed interpretation of experiments and open up the path to characterizing more complex scenarios, such as probing the surface of oxide-based catalysts with high specificity under operando conditions (e.g., using diffuse reflectance infrared Fourier transform spectroscopy, or DRIFTS), where changes in particle shape and faceting might occur.

SUPPLEMENTARY MATERIAL

The supplementary material includes top and side views of the unrelaxed ceria surfaces; details of the computations; and a comparison of the optimized structures of CO adsorption on the oxidized and reduced ceria surfaces obtained with the PBE+U and HSE06 approaches.

ACKNOWLEDGMENTS

This project received funding from the European Union's Horizon 2020 research and innovation program under the Marie Skłodowska-Curie Grant Agreement No. 832121, the Deutsche Forschungsgemeinschaft (DFG, German Research Foundation)—Project No. 426888090—SFB 1441, and the National Natural Science Foundation of China (21902005). M.V.G.-P. acknowledges the support by the MICINN-Spain (Grant Nos. RTI2018-101604-B-I00 and PID2021-128915NB-I00) and the International Excellence Fellowship of Karlsruhe Institute of Technology (KIT) funded within the Framework of the University of Excellence Concept “The Research University in the Helmholtz Association I Living the Change” Germany. Computer time provided by FinisTerra3 at CESGA (Centro de Supercomputación de Galicia) and the RES (Red Española de Supercomputación) resources at MareNostrum 4 (BSC, Barcelona) and LaPalma (IAC, Canarias) nodes is acknowledged.

AUTHOR DECLARATIONS

Conflict of Interest

The authors have no conflicts to disclose.

Author Contributions

Pablo G. Lustemberg and Chengwu Yang contributed equally to this work.

Pablo G. Lustemberg: Investigation (lead); Writing – review & editing (equal). **Chengwu Yang:** Investigation (lead); Writing – review & editing (equal). **Yuemin Wang:** Supervision (lead); Writing – review & editing (equal). **Christof Wöll:** Conceptualization

(lead); Supervision (lead); Writing – original draft (lead); Writing – review & editing (equal). **M. Verónica Ganduglia-Pirovano:** Conceptualization (lead); Supervision (lead); Writing – original draft (lead); Writing – review & editing (equal).

DATA AVAILABILITY

The data that support the findings of this study are openly available in Materials Cloud (<https://www.materialscloud.org/home>) at <http://doi.org/10.24435/materialscloud:7n-7m>.

REFERENCES

- ¹A. Trovarelli and P. Fornasiero, *Catalysis by Ceria and Related Materials* (Imperial College Press, London, UK, 2002).
- ²S. Park, J. M. Vohs, and R. J. Gorte, “Direct oxidation of hydrocarbons in a solid-oxide fuel cell,” *Nature* **404**(6775), 265–267 (2000).
- ³C. Xu and X. Qu, “Cerium oxide nanoparticle: A remarkably versatile rare earth nanomaterial for biological applications,” *NPG Asia Mater.* **6**(3), e90 (2014).
- ⁴W. Huang and Y. Gao, “Morphology-dependent surface chemistry and catalysis of CeO₂ nanocrystals,” *Catal. Sci. Technol.* **4**(11), 3772–3784 (2014).
- ⁵A. Trovarelli and J. Llorca, “Ceria catalysts at nanoscale: How do crystal shapes shape catalysis?,” *ACS Catal.* **7**(7), 4716–4735 (2017).
- ⁶Z. Hu, X. Liu, D. Meng, Y. Guo, Y. Guo, and G. Lu, “Effect of ceria crystal plane on the physicochemical and catalytic properties of Pd/ceria for CO and propane oxidation,” *ACS Catal.* **6**(4), 2265–2279 (2016).
- ⁷G. Vilé, S. Colussi, F. Krumeich, A. Trovarelli, and J. Pérez-Ramírez, “Opposite face sensitivity of CeO₂ in hydrogenation and oxidation catalysis,” *Angew. Chem., Int. Ed.* **53**(45), 12069–12072 (2014).
- ⁸Y. Cao, L. Zhao, T. Gutmann, Y. Xu, L. Dong, G. Buntkowsky, and F. Gao, “Getting insights into the influence of crystal plane effect of shaped ceria on its catalytic performances,” *J. Phys. Chem. C* **122**(35), 20402–20409 (2018).
- ⁹C. Li, Y. Sun, I. Djerdj, P. Voepel, C.-C. Sack, T. Weller, R. Ellinghaus, J. Sann, Y. Guo, B. M. Smarsly, and H. Over, “Shape-controlled CeO₂ nanoparticles: Stability and activity in the catalyzed HCl oxidation reaction,” *ACS Catal.* **7**(10), 6453–6463 (2017).
- ¹⁰I. Florea, C. Feral-Martin, J. Majimel, D. Ithiawakrim, C. Hirlimann, and O. Ersen, “Three-dimensional tomographic analyses of CeO₂ nanoparticles,” *Cryst. Growth Des.* **13**(3), 1110–1121 (2013).
- ¹¹J. Chen, X.-P. Wu, M. A. Hope, K. Qian, D. M. Halat, T. Liu, Y. Li, L. Shen, X. Ke, Y. Wen, J.-H. Du, P. C. M. M. Magusin, S. Paul, W. Ding, X.-Q. Gong, C. P. Grey, and L. Peng, “Polar surface structure of oxide nanocrystals revealed with solid-state NMR spectroscopy,” *Nat. Commun.* **10**(1), 5420 (2019).
- ¹²C. Yang, X. Yu, S. Heißler, A. Nefedov, S. Colussi, J. Llorca, A. Trovarelli, Y. Wang, and C. Wöll, “Surface faceting and reconstruction of ceria nanoparticles,” *Angew. Chem., Int. Ed.* **56**(1), 375–379 (2017).
- ¹³P. A. Crozier, R. Wang, and R. Sharma, “In situ environmental TEM studies of dynamic changes in cerium-based oxides nanoparticles during redox processes,” *Ultramicroscopy* **108**(11), 1432–1440 (2008).
- ¹⁴O. S. Bezkravnyi, P. Kraszkiewicz, M. Ptak, and L. Kepinski, “Thermally induced reconstruction of ceria nanocubes into zigzag {111}-nanofaceted structures and its influence on catalytic activity in CO oxidation,” *Catal. Commun.* **117**, 94–98 (2018).
- ¹⁵P. Perez-Bailac, P. G. Lustemberg, and M. V. Ganduglia-Pirovano, “Facet-dependent stability of near-surface oxygen vacancies and excess charge localization at CeO₂ surfaces,” *J. Phys.: Condens. Matter* **33**(50), 504003 (2021).
- ¹⁶C. Wöll, “Structure and chemical properties of oxide nanoparticles determined by surface-ligand IR spectroscopy,” *ACS Catal.* **10**(1), 168–176 (2020).
- ¹⁷Y. Wang and C. Wöll, “IR spectroscopic investigations of chemical and photochemical reactions on metal oxides: Bridging the materials gap,” *Chem. Soc. Rev.* **46**(7), 1875–1932 (2017).
- ¹⁸M. Xu, H. Noei, K. Fink, M. Muhler, Y. Wang, and C. Wöll, “The surface science approach for understanding reactions on oxide powders: The importance of IR spectroscopy,” *Angew. Chem., Int. Ed.* **51**(19), 4731–4734 (2012).

- ¹⁹G. Pacchioni, "Quantum chemistry of oxide surfaces: From CO chemisorption to the identification of the structure and nature of point defects on MgO," *Surf. Rev. Lett.* **07**(03), 277–306 (2000).
- ²⁰M. I. Zaki, B. Vielhaber, and H. Knoezinger, "Low-temperature carbon monoxide adsorption and state of molybdena supported on alumina, titania, ceria, and zirconia. An infrared spectroscopic investigation," *J. Phys. Chem.* **90**(14), 3176–3183 (1986).
- ²¹C. Li, Y. Sakata, T. Arai, K. Domen, K.-i. Maruya, and T. Onishi, "Carbon monoxide and carbon dioxide adsorption on cerium oxide studied by Fourier-transform infrared spectroscopy. Part 1.—Formation of carbonate species on dehydroxylated CeO₂, at room temperature," *J. Chem. Soc., Faraday Trans. 1* **85**(4), 929–943 (1989).
- ²²C. Binet, M. Daturi, and J.-C. Lavalley, "IR study of polycrystalline ceria properties in oxidised and reduced states," *Catal. Today* **50**(2), 207–225 (1999).
- ²³R. Farra, S. Wrabetz, M. E. Schuster, E. Stotz, N. G. Hamilton, A. P. Amrute, J. Pérez-Ramírez, N. López, and D. Teschner, "Understanding CeO₂ as a Deacon catalyst by probe molecule adsorption and in situ infrared characterisations," *Phys. Chem. Chem. Phys.* **15**(10), 3454–3465 (2013).
- ²⁴S. Agarwal, X. Zhu, E. J. M. Hensen, B. L. Mojet, and L. Lefferts, "Surface-dependence of defect chemistry of nanostructured ceria," *J. Phys. Chem. C* **119**(22), 12423–12433 (2015).
- ²⁵C. Li, Y. Sakata, T. Arai, K. Domen, K.-I. Maruya, and T. Onishi, "Adsorption of carbon monoxide and carbon dioxide on cerium oxide studied by Fourier-transform infrared spectroscopy. Part 2.—Formation of formate species on partially reduced CeO₂ at room temperature," *J. Chem. Soc., Faraday Trans. 1* **85**(6), 1451–1461 (1989).
- ²⁶G. A. H. Mekheimer and M. I. Zaki, "Low-temperature IR spectroscopy of CO adsorption on calcined supported CeO₂: Probing adsorbed species and adsorbing sites," *Adsorpt. Sci. Technol.* **15**(5), 377–389 (1997).
- ²⁷H. V. Thang, F. Maleki, S. Tosoni, and G. Pacchioni, "Vibrational properties of CO adsorbed on Au single atom catalysts on TiO₂(101), ZrO₂(101), CeO₂(111), and LaFeO₃(001) surfaces: A DFT study," *Top. Catal.* **65**(17), 1573–1586 (2022).
- ²⁸A. Gil, A. Clotet, J. M. Ricart, G. Kresse, M. G. Hernández, N. Rösch, and P. Sautet, "Site preference of CO chemisorbed on Pt(111) from density functional calculations," *Surf. Sci.* **530**(1–2), 71–87 (2003).
- ²⁹P. G. Lustemberg, P. N. Plessow, Y. Wang, C. Yang, A. Nefedov, F. Studt, C. Wöll, and M. V. Ganduglia-Pirovano, "Vibrational frequencies of cerium-oxide-bound CO: A challenge for conventional DFT methods," *Phys. Rev. Lett.* **125**(25), 256101 (2020).
- ³⁰A. V. Krukau, O. A. Vydrov, A. F. Izmaylov, and G. E. Scuseria, "Influence of the exchange screening parameter on the performance of screened hybrid functionals," *J. Chem. Phys.* **125**(22), 224106 (2006).
- ³¹C. Yang, L.-L. Yin, F. Bebenese, M. Buchholz, H. Sezen, S. Heissler, J. Chen, A. Nefedov, H. Idriss, X.-Q. Gong, and C. Wöll, "Chemical activity of oxygen vacancies on ceria: A combined experimental and theoretical study on CeO₂(111)," *Phys. Chem. Chem. Phys.* **16**(44), 24165–24168 (2014).
- ³²C. Yang, X. Yu, S. Heissler, P. G. Weidler, A. Nefedov, Y. Wang, C. Wöll, T. Kropp, J. Paier, and J. Sauer, "O₂ activation on ceria catalysts—The importance of substrate crystallographic orientation," *Angew. Chem., Int. Ed. Engl.* **56**(51), 16399–16404 (2017).
- ³³C. Yang, M. Capdevila-Cortada, C. Dong, Y. Zhou, J. Wang, X. Yu, A. Nefedov, S. Heissler, N. López, W. Shen, C. Wöll, and Y. Wang, "Surface refaceting mechanism on cubic ceria," *J. Phys. Chem. Lett.* **11**(18), 7925–7931 (2020).
- ³⁴M. C. Payne, M. P. Teter, D. C. Allan, T. A. Arias, and J. D. Joannopoulos, "Iterative minimization techniques for ab initio total-energy calculations: Molecular dynamics and conjugate gradients," *Rev. Mod. Phys.* **64**(4), 1045–1097 (1992).
- ³⁵G. Kresse and J. Furthmüller, "Efficient iterative schemes for ab initio total-energy calculations using a plane-wave basis set," *Phys. Rev. B* **54**(16), 11169–11186 (1996).
- ³⁶G. Kresse and J. Hafner, "Ab initio molecular dynamics for liquid metals," *Phys. Rev. B* **47**(1), 558–561 (1993).
- ³⁷S. L. Dudarev, G. A. Botton, S. Y. Savrasov, C. J. Humphreys, and A. P. Sutton, "Electron-energy-loss spectra and the structural stability of nickel oxide: An LSDA+U study," *Phys. Rev. B* **57**(3), 1505–1509 (1998).
- ³⁸S. Fabris, S. de Gironcoli, S. Baroni, G. Vicario, and G. Balducci, "Taming multiplicity with density functionals: A case study of defective ceria," *Phys. Rev. B* **71**(4), 041102 (2005).
- ³⁹M. Cococcioni and S. de Gironcoli, "Linear response approach to the calculation of the effective interaction parameters in the LDA+U method," *Phys. Rev. B* **71**(3), 035105 (2005).
- ⁴⁰J. P. Perdew, K. Burke, and M. Ernzerhof, "Generalized gradient approximation made simple," *Phys. Rev. Lett.* **77**(18), 3865–3868 (1996).
- ⁴¹J. L. F. Da Silva, M. V. Ganduglia-Pirovano, J. Sauer, V. Bayer, and G. Kresse, "Hybrid functionals applied to rare-earth oxides: The example of ceria," *Phys. Rev. B* **75**(4), 045121 (2007).
- ⁴²D. Du, M. J. Wolf, K. Hermansson, and P. Broqvist, "Screened hybrid functionals applied to ceria: Effect of Fock exchange," *Phys. Rev. B* **97**(23), 235203 (2018).
- ⁴³M. V. Ganduglia-Pirovano, J. L. F. Da Silva, and J. Sauer, "Density-functional calculations of the structure of near-surface oxygen vacancies and electron localization on CeO₂(111)," *Phys. Rev. Lett.* **102**(2), 026101 (2009).
- ⁴⁴J. Paier, C. Penschke, and J. Sauer, "Oxygen defects and surface chemistry of ceria: Quantum chemical studies compared to experiment," *Chem. Rev.* **113**(6), 3949–3985 (2013).
- ⁴⁵J. Graciani, A. M. Márquez, J. J. Plata, Y. Ortega, N. C. Hernández, A. Meyer, C. M. Zicovich-Wilson, and J. F. Sanz, "Comparative study on the performance of hybrid DFT functionals in highly correlated oxides: The case of CeO₂ and Ce₂O₃," *J. Chem. Theory Comput.* **7**(1), 56–65 (2011).
- ⁴⁶J. Sauer, P. Ugliengo, E. Garrone, and V. R. Saunders, "Theoretical study of van der Waals complexes at surface sites in comparison with the experiment," *Chem. Rev.* **94**(7), 2095–2160 (1994).
- ⁴⁷F. R. Rehak, G. Piccini, M. Alessio, and J. Sauer, "Including dispersion in density functional theory for adsorption on flat oxide surfaces, in metal–organic frameworks and in acidic zeolites," *Phys. Chem. Chem. Phys.* **22**, 7577–7585 (2020).
- ⁴⁸H. J. Monkhorst and J. D. Pack, "Special points for Brillouin-zone integrations," *Phys. Rev. B* **13**(12), 5188–5192 (1976).
- ⁴⁹Y. Pan, N. Nilius, C. Stiehler, H.-J. Freund, J. Goniakowski, and C. Noguera, "Ceria nanocrystals exposing wide (100) facets: Structure and polarity compensation," *Adv. Mater. Interfaces* **1**(9), 1400404 (2014).
- ⁵⁰M. Capdevila-Cortada and N. López, "Entropic contributions enhance polarity compensation for CeO₂(100) surfaces," *Nat. Mater.* **16**(3), 328–334 (2017).
- ⁵¹O. Matz and M. Calatayud, "Breaking H₂ with CeO₂: Effect of surface termination," *ACS Omega* **3**(11), 16063–16073 (2018).
- ⁵²D. Porezag and M. R. Pederson, "Infrared intensities and Raman-scattering activities within density-functional theory," *Phys. Rev. B* **54**(11), 7830–7836 (1996).
- ⁵³M. Huang and S. Fabris, "CO adsorption and oxidation on ceria surfaces from DFT+U calculations," *J. Phys. Chem. C* **112**(23), 8643–8648 (2008).
- ⁵⁴M. Nolan and G. W. Watson, "The surface dependence of CO adsorption on ceria," *J. Phys. Chem. B* **110**(33), 16600–16606 (2006).
- ⁵⁵Z. Yang, T. K. Woo, and K. Hermansson, "Strong and weak adsorption of CO on CeO₂ surfaces from first principles calculations," *Chem. Phys. Lett.* **396**(4–6), 384–392 (2004).
- ⁵⁶B. Herschend, M. Baudin, and K. Hermansson, "CO adsorption on CeO₂(110) using hybrid-DFT embedded-cluster calculations," *Chem. Phys.* **328**, 345–353 (2006).
- ⁵⁷C. Müller, B. Herschend, K. Hermansson, and B. Paulus, "Application of the method of increments to the adsorption of CO on the CeO₂ (110) surface," *J. Chem. Phys.* **128**(21), 214701 (2008).